13

Inverse Analysis Applied to Mushy Steel Rheological Properties Testing Using Hybrid Numerical-Analytical Model

Miroslaw Glowacki
AGH University of Science and Technology
Poland

1. Introduction

Integrated casting and rolling technologies are most recent and very efficient way of hot strip production. More and more companies all over the world are able to manage such processes. The mentioned technologies ensure huge reduction of rolling costs, very high product quality and low investment costs. Computer simulation is of vital importance to the development of "know how" theory for these processes. The lack of publications concerning mechanical properties and behaviour of steels simultaneously subjected to both plastic deformation and solidification was the inspiration for the investigation. This also necessitated the development of an appropriate mathematical model of mushy-steel deformation. The contribution summarizes the results of the author's recent theoretical research concerning the computer simulation of mushy steel published in recent years in well-known journals and book chapters [Glowacki, 2006; Glowacki at al., 2010; Glowacki & Hojny, 2006, 2009; Hojny & Glowacki, 2008, 2009a, 2009b, 2011; Hojny at al., 2009].

As an example of a company providing the integrated casting and rolling technologies one can mention the plant located in Cremona, Italy which develops the new methods of steel strip manufacturing. They are called Inline Strip Production (ISP) and Arvedi Steel Technology (AST) processes and are characterized by very high temperature allowed at the mill entry. The instant rolling of slabs which leave the casting machine allows for the utilization of the heat stored in the strips during inline casting. Both the mentioned technologies ensure huge reduction of rolling forces and their details are usually classified.

The development of "know how" theory for the semi-solid steel rolling technology requires numerical modelling. The development of appropriate mathematical models is limited by the lack of thermal and mechanical properties concerning mushy steels deformation in temperature range which is close to solidus line. The work presented in the current contribution is an attempt to cover the gap providing a proposition of a hybrid numerical-analytical model of semi-solid steel deformation. The mathematical modelling of steel deformation in semi-solid state, as well as experimental work in this field, are innovative topics regarding the very high temperature range deformation processes. Tracing the related papers published in the past 10 years one can find many dealings with experimental results for non-ferrous metals tests (Kang & Yoon, 1997; Koc at al., 1996; Kopp at al., 2003; Sang-

Yong at al., 2001; Zhao at al., 2006). The first results regarding steel deformation at extra high temperature were presented during last few years (Li, 2005; Seol, 1999, 2002). Most of the problems concerning semi-solid steel testing are caused by the very high level of steel liquidus and solidus temperatures in comparison with non-ferrous metals. The deformation tests for non-ferrous metals are much easier. The rising abilities of thermo-mechanical simulators enable investigation of steel samples and as a result both computer simulation and the development of new, very high temperature rolling technologies like Arvedi ISP and AST processes. The lack of mathematical models describing the steel behaviour in the last phase of solidification with simultaneous plastic deformation was the inspiration of the investigation described in the proposed book chapter.

The main goal of the chapter is to present problems of theoretical work leading to the development of a methodology of very high temperature testing of steel samples while their central parts are still mushy. In such conditions the deformation of samples is strongly inhomogeneous and all the well-known methods of yield stress curve examination fail due to significant barrelling of the sample. Although the investigation concerned both physical tests and dedicated simulation system, the author sacrifices the contribution to the hybrid model which is the heart of the system. With the help of inverse analysis it allows for the right interpretation of deformation tests providing data regarding the mushy steel rheological properties.

2. Physical basis and characteristic features of steel deformed at very high temperature

The rolling equipment for the ISP process allows for reduction of initial mould strip thickness from 74 mm to 55 mm during liquid core reduction process. The region of maximum strip temperature for a high reduction mill is located in the strip centre and varies from 1220 °C to 1375 °C depending on the casting speed. The main benefits of the technology are: inverse temperature gradient, good product quality, very low level of heating energy consumption, up to 20 times lower water consumption in comparison to traditional rolling, low level of installed mill power, compact rolling equipment layout, no need for tunnel furnace and very low investment costs. The AST technology is a result of further development of ISP into a real endless process and the benefits of its application are even greater. The whole reduction process is running in one rolling mill consisting of 5 or 7 stands, which can reduce the strip thickness from 55÷70 mm to 0.8 mm. The maximum temperature of the strip occurs in central region of its cross-section and varies from 1340 °C to 1420 °C depending on the casting speed. This suggests that the central region of the strand subjected to the rolling is still mushy.

The main benefits of the new very high temperature technologies are significantly lower rolling forces and very favourable temperature field inside the steel plate. However, certain problems arise which are specific for this kind of metal treatment. The central parts of slabs are mushy and the solidification is not yet finished while the deformation is in progress. This results in changes in material density and occurrence of characteristic temperatures having great influence on the plastic behaviour of the material (Senk, 2000; Suzuki, 1988). The nil strength temperature (NST), strength recovery temperature (SRT), nil ductility temperature (NDT) and ductility recovery temperature (DRT) have effect on steel plastic

behaviour and limit plastic deformation. The Nil Strength Temperature (NST) is the temperature level at which material strength drops to zero while the steel is being heated above the solidus temperature. Another temperature associated with NST is the Strength Recovery Temperature (SRT). At this temperature the cooled material regains strength greater than 0.5 N/mm2. Nil Ductility Temperature (NDT) represents the temperature at which the heated steel loses its ductility. The Ductility Recovery Temperature (DRT) is the temperature at which the ductility of the material (characterised by reduction of area) reaches 5% while it is being cooled. Over this temperature the plastic deformation is not allowed at any stress tensor configuration.

Significant changes of density and lack of data regarding material's thermal and mechanical properties are vital problems of the modelling. They have great influence on steel rheology and heat transfer. An issue of great importance is the lack of strain-stress relationships, which in the temperature range above 1400 ˚C strongly depend on the density and are very temperature sensitive. It is not easy to run isothermal tests that could be the source of the computation of yield stress function parameters for such high temperatures. There are also some problems with the interpretation of tests results.

Density is very important for plastic behaviour of mushy steel plates. It varies with temperature and depends on the cooling rate. The solidification process causes non-uniform density distribution in the controlled volume resulting in non-uniform deformation and heat conduction. There are three main factors causing density changes: solid phase formation, thermal shrinkage and movement of liquid particles inside the solid skeleton. The density plays an important role in both mechanical and thermal solutions.

The contribution sheds some light on the physical problems but it focuses on the axial-symmetrical computer model, which ensures the right simulation of mushy steel samples deformation reflecting the physical requirements. The presented model fills the gap in modelling of plastic behaviour of semi-solid steels.

3. Hybrid numerical-analytical model of mushy steel deformation

Testing of steels at temperature higher than 1400 ˚C is difficult due to deformation instability and risk of sample damage during experiment. Such experiments do not assure the strain homogeneity and cannot be interpreted using traditional methods. Appropriate interpretation of the results is possible only with the help of a computer aided engineering system. The contribution reports a new model underlying such a system developed by the author's team. Together with GLEEBLE physical simulator equipped with high temperature module the code allows for investigation of properties of semi-solid steel.

The numerical solver is the less visible yet very powerful kernel of the system. It is based on a thermal-mechanical model with variable density. The mechanical part of the model is a hybrid variational solution with analytical mass conservation condition constraining the velocity field components. The accuracy of the proposed solution is very good due to negligible volume loss guaranteed by the analytical form of the mass conservation condition. This is important for materials with variable density and is not captured by classical solutions. Analytical condition eliminates problems with unintentional specimen volume changes caused by application of numerical methods. The existing, physical changes of steel density in the mushy zone have influence on real variations of controlled volume.

On the other hand numerical errors can be a source of volume loss which interferes with real changes. This effect is very undesirable in modelling of thermal-mechanical behaviour of steel in temperature range characteristic for the (transformation of state of aggregation).

The mentioned mechanical and thermal parts of the mathematical model of the process are supported by a third one, i.e. the density changes model. The mechanical part is responsible for the strain, strain rate and stress distribution in a controlled volume.

4. Thermal part of the model

Heat exchange between solid metal and environment, and its flow inside the metal is controlled by a number of factors. During phase change two additional phenomena have to be taken into account. Note that in the process of deformation of steel at temperature of liquid to solid phase transition there are two sources of heat changes. On the one hand heat is generated due to the state transformation. On the other hand it is secreted as a result of plastic deformation. In addition, steel density variations also cause changes of body temperature.

Thermal solution has a major impact on simulation results, since the temperature has strong effect on remaining variables. This is especially evident if the specimen temperature is close to solidus line when the body consist of both solid and semi-solid regions. In such case the affected phenomena are: plastic flow of solid and mushy materials, stress evolution and density changes. The theoretical temperature field is a solution of Fourier-Kirchhoff equation with appropriate boundary conditions.

The most general form of the Fourier-Kirchhoff equation in any coordinate system can be written in operator form as follows:

$$\nabla^T(\mathbf{\Lambda}\,\nabla T) + Q = c_p\rho\left(\boldsymbol{v}^{\boldsymbol{T}}\nabla T + \frac{\partial T}{\partial \tau}\right) \tag{1}$$

where T is the temperature distribution in the controlled volume and $\mathbf{\Lambda}$ denotes the symmetrical second order tensor called heat transformation tensor. In case of thermal inhomogeneity the whole tensor has to be considered. Q represents the rate of heat generation (or consumption) due to the phase transformation, due to plastic work done and due to electric current flow (resistance heating of the sample is usually applied). Finally c_p describes the specific heat, ρ the steel density, $\boldsymbol{v}$ the velocity vector of specimen particles and τ the elapsed time. The heat transformation tensor consists of a set of anisotropic heat transformation coefficients and can be given in a form:

$$\mathbf{\Lambda} = \begin{pmatrix} \lambda_{xx} & \lambda_{xy} & \lambda_{xz} \\ \lambda_{yx} & \lambda_{yy} & \lambda_{yz} \\ \lambda_{zx} & \lambda_{zy} & \lambda_{zz} \end{pmatrix} \tag{2}$$

In the case of anisotropic bodies, the solution is carried out locally, and the axes of coordinate system are oriented in accordance with the principal directions of the thermal conductivity. In this case all off-diagonal components of the heat transformation tensor are zeros ($\lambda_{ij} = 0,\ i \neq j$) and equation (2) becomes:

$$\mathbf{\Lambda} = \begin{pmatrix} \lambda_{xx} & 0 & 0 \\ 0 & \lambda_{yy} & 0 \\ 0 & 0 & \lambda_{zz} \end{pmatrix} \tag{3}$$

Furthermore for a thermally isotropic material $\lambda_{xx} = \lambda_{yy} = \lambda_{zz} = \lambda$ and tensor of the heat transformation can be written in the index notation can be as:

$$\Lambda_{ij} = \lambda \delta_{ij} \tag{4}$$

where δ_{ij} is the Kronecker delta.

The temperature of samples compressed in axially-symmetric process can be determined by solving the appropriate form of Fourier-Kirchhoff equation. Here the equation will be expressed in the cylindrical coordinate system, which is a natural choice for the cylindrically-shaped samples. It takes following differential form:

$$\frac{1}{r}\frac{\partial}{\partial r}\left(r\lambda_r \frac{\partial T}{\partial r}\right) + \frac{1}{r}\frac{\partial}{\partial \theta}\left(\frac{1}{r}\lambda_\theta \frac{\partial T}{\partial \theta}\right) + \frac{\partial}{\partial z}\left(\lambda_z \frac{\partial T}{\partial z}\right) + Q = \rho c_p \frac{\partial T}{\partial \tau} \tag{5}$$

The assumption of axial symmetry can be considered appropriate for the tensile and compression tests of steel in semi-solid state in all physically stable cases. It is invalid only for failed experiments. The symmetry simplifies the model by implying identical temperature distribution at any axial sample cross-section. This results in the equation:

$$\frac{\partial T}{\partial \theta} = 0 \tag{6}$$

Equation (5) can be further simplified if the heat properties of the medium are assumed isotropic. By calculating the differentials in equation (5) and using equation (6) we get the following form of Fourier-Kirchhoff equations for isotropic, axially-symmetric heat flow:

$$\lambda\left(\frac{\partial^2 T}{\partial r^2} + \frac{1}{r}\frac{\partial T}{\partial r} + \frac{\partial^2 T}{\partial z^2}\right) + Q = \rho c_p \frac{\partial T}{\partial \tau} \tag{7}$$

Equation (7) needs to be solved with appropriate initial and boundary conditions. The initial conditions relate to cases of non-stationary heat exchange. Most solutions use Cauchy condition which assume the known a priori temperature distribution at time τ_0: $T_\Omega(\tau_0) = f_\Omega$. In a particular (but often adopted) case the temperature is assumed to be constant throughout the considered area $T_\Omega(\tau_0) = T_0 = const$.

Boundary conditions have more complex nature and relate to all cases of heat transfer and describe the spatial aspect of the heat exchange. The considered continuous medium changes its temperature though convection, radiation, conduction, or a combination of these phenomena. Theoretical solutions of the problem are generally subject to one or more boundary conditions. Combined Hankel's boundary conditions have been adopted for the presented model. The conditions for axially-symmetrical problem can be written in form of a differential equation:

$$\lambda r \frac{\partial T}{\partial n} + \alpha(T - T_0) + q = 0 \tag{8}$$

In equation (8) T_0 is the distribution of border temperature, q describes the heat flux through the boundary of the deformation zone, α is the heat transfer coefficient and n is a vector which is normal to the boundary surface. More details concerning the problem can be found in (Glowacki, 1996). Equation (7) subject to condition (8) defines the problem of temperature evolution during the whole process of heating and deformation of the samples.

Note that (7) is a spatiotemporal equation. The solution of such equations is difficult because in general case the temperature is a function of both location (r, z) and time τ.

$$T = T(r, z, \tau) \tag{9}$$

In addition, the used boundary conditions, appropriate for the cooling or heating of the sample are also described by differential equation. For that reason equation (7) is solved in a two-step process (Zienkiewicz at al., 2005):

- the corresponding steady-state equation is solved. After FEM discretization this yields a matrix algebraic equation,
- the solution obtained in the first step is then adapted to non-steady-state conditions using a transient discretization of the time variable.

4.1 Thermal model for steady-state heat flow process

The Fourier-Kirchhof equation (7) for the steady heat flow can be written as:

$$\lambda\left(\frac{\partial^2 T}{\partial r^2} + \frac{1}{r}\frac{\partial T}{\partial r} + \frac{\partial^2 T}{\partial z^2}\right) + Q = 0 \tag{10}$$

Application of finite element method for solving problems of heat flow requires a functional. Equation (10) together with the boundary conditions given by equation (8) needs to be expressed in a variational setting.

Consider the problem of optimizing the general form of the heat flux power functional.

$$\chi = \int_V f(r, z, T, T_r, T_z)\ dV + \int_S \left(qT + \frac{1}{2}\alpha(T - T_0)^2\right)\ dS \tag{11}$$

where f is a function of position, temperature and temperature gradient:

$$T_r = \frac{\partial T}{\partial r}; \qquad T_z = \frac{\partial T}{\partial z} \tag{12}$$

This function is specified in the relevant domain V with the boundary S. Let us consider a small variation of the functional (11):

$$\delta\chi = \int_V \left(\frac{\partial f}{\partial T}\delta T + \frac{\partial f}{\partial T_r}\delta T_r + \frac{\partial f}{\partial T_z}\delta T_z\right) dV + \int_S [q\delta T + \alpha(T - T_0)\ \delta T] dS \tag{13}$$

that can be rewritten as:

$$\delta\chi = \int_V \delta T \left[\frac{\partial f}{\partial T} - \frac{\partial}{\partial r}\left(\frac{\partial f}{\partial T_r}\right) - \frac{\partial}{\partial z}\left(\frac{\partial f}{\partial T_z}\right)\right] dV + \int_S \delta T \left(q + \alpha(T - T_0) + l_r \frac{\partial f}{\partial T_r} + l_z \frac{\partial f}{\partial T_z}\right) dS \quad (14)$$

where l_r and l_z are the direction cosines of normal to the outer surface with respect to Or and Oz axes, respectively.

A necessary condition for the functional (11) to reach extreme value for a given function is for the variation $\delta\chi$ to be equal to 0. Since equation (14) must be satisfied for any variation δT, the expressions in brackets have to be zero at an extreme:

$$\frac{\partial}{\partial r}\left(\frac{\partial f}{\partial T_r}\right) + \frac{\partial}{\partial z}\left(\frac{\partial f}{\partial T_z}\right) - \frac{\partial f}{\partial T} = 0 \quad (15)$$

for the entire volume V and

$$l_x \frac{\partial f}{\partial T_x} + l_z \frac{\partial f}{\partial T_z} + q + \alpha(T - T_0) = 0 \quad (16)$$

for its boundary S. Can therefore be concluded that if one satisfy the equations (15) and (16) than the functional (11) reaches an optimum. Both of these formulations are equivalent. The above reasoning is the solution of so called Euler problem. In the presented particular case the appropriate form of the function f is as follows:

$$f = r\left[\frac{1}{2}\lambda(T_r^2 + T_z^2) - QT\right] \quad (17)$$

where T_r and T_z are given by relationships (12). In this case the equations (15) and (16) can be written as follows:

$$\begin{aligned} \lambda\left(\frac{\partial^2 T}{\partial r^2} + \frac{1}{r}T_r + \frac{\partial^2 T}{\partial z^2}\right) + Q = 0 \\ \lambda r \frac{\partial T}{\partial n} + q + \alpha(T - T_0) = 0 \end{aligned} \quad (18)$$

The presented reasoning shows that the assumption of steady-state heat flow leads to equations (18). The first of them is identical with the equation (10), and the second to boundary condition (8). Thus, according to the Euler reasoning, the solution of equation (10) satisfying the boundary condition (8) is the functional extremal:

$$\chi = \int_V r\left\{\frac{1}{2}\lambda\left[\left(\frac{\partial T}{\partial r}\right)^2 + \left(\frac{\partial T}{\partial z}\right)^2\right] - QT\right\} dV + \int_S \left(qT + \frac{1}{2}\alpha(T - T_0)^2\right) dS \quad (19)$$

Optimization of the functional (19) in the domain of discrete functions is based on replacement of the continuous real function of the temperature distribution $T(r,z)$ by their discrete counterparts. In the proposed solution the finite element method was used for that purpose. The discretization of the control volume was done accordingly. The temperature distribution function was discretized according to the formula:

$$T(r,z) = \mathbf{n}^{\boldsymbol{T}}(r,z)\,\mathbf{T} \tag{20}$$

where $\mathbf{n}(r,z)$ is a vector of the shape function and $\mathbf{T}$ is a nodal temperature vector. After substituting (20) and its derivatives to (19) it takes the discrete form:

$$\chi = \int_V r\left\{\frac{1}{2}\lambda\left[\left(\frac{\partial \mathbf{n}^T}{\partial r}\mathbf{T}\right)^2 + \left(\frac{\partial \mathbf{n}^T}{\partial z}\mathbf{T}\right)^2\right] - Q\mathbf{n}^{\boldsymbol{T}}\mathbf{T}\right\}dV + \int_S\left(q\mathbf{n}^{\boldsymbol{T}}\mathbf{T} + \frac{1}{2}\alpha(\mathbf{n}^{\boldsymbol{T}}\mathbf{T} - T_0)^2\right)dS \tag{21}$$

From the mathematical point of view, equation (21) no longer defines a functional, but a function of many variables. Nevertheless hereinafter it still will be referred to as a functional. Its derivative with respect to $\mathbf{T}$ is given as follows:

$$\frac{\partial \chi}{\partial \mathbf{T}} = \int_V r\left[\lambda\mathbf{T}^{\boldsymbol{T}}\left(\frac{\partial \mathbf{n}}{\partial r}\frac{\partial \mathbf{n}^T}{\partial r} + \frac{\partial \mathbf{n}}{\partial z}\frac{\partial \mathbf{n}^T}{\partial z}\right) - \mathrm{Q}\mathbf{n}^T\right]dV + \int_S(q\mathbf{n}^T + \alpha(\mathbf{T}^{\boldsymbol{T}}\mathbf{n} - T_0)\mathbf{n}^T)dS \tag{22}$$

Equation (22) one can written in matrix form as:

$$\mathbf{HT} + \mathbf{p} = \mathbf{0} \tag{23}$$

where matrix $\mathbf{H}$ and vector $\mathbf{p}$ have shapes:

$$\begin{aligned}\mathbf{H} &= \int_V r\lambda\left(\frac{\partial \mathbf{n}}{\partial r}\frac{\partial \mathbf{n}^T}{\partial r} + \frac{\partial \mathbf{n}}{\partial z}\frac{\partial \mathbf{n}^T}{\partial z}\right)dV + \int_S \alpha\mathbf{n}\mathbf{n}^T dS \\ \mathbf{p} &= -\int_V rQ\mathbf{n}\ dV - \int_S(\alpha T_0 - q)\,\mathbf{n}\ dS\end{aligned} \tag{24}$$

The system of linear equations (23) can be solved using standard methods of linear algebra. This yields the discrete temperature vector $\mathbf{T}$.

4.2 Thermal model for non-steady-state heat flow

For the non-steady-state heat flow equation (7) has to be used instead of equation (10). A derivation similar to the one for the steady-state flow and the same space discretization lead to formulation of discrete form of functional equivalent to equation (7). It is analogous to functional (21).

$$\begin{aligned}\chi = \int_V r\left\{\frac{1}{2}\lambda\left[\left(\frac{\partial \mathbf{n}^T}{\partial r}\mathbf{T}\right)^2 + \left(\frac{\partial \mathbf{n}^T}{\partial z}\mathbf{T}\right)^2\right] - \left[Q - \rho c_p\frac{\partial}{\partial \tau}(\mathbf{n}^{\boldsymbol{T}}\mathbf{T})\right]\mathbf{n}^{\boldsymbol{T}}\mathbf{T}\right\}dV + \\ + \int_S\left(q\mathbf{n}^{\boldsymbol{T}}\mathbf{T} + \frac{1}{2}\alpha(\mathbf{n}^{\boldsymbol{T}}\mathbf{T} - T_0)^2\right)dS\end{aligned} \tag{25}$$

Differentiation of functional (25) with respect to $\mathbf{T}$ leads to relation which is similar to (22).

$$\frac{\partial \chi}{\partial \mathbf{T}} = \int_V r\left[\lambda \mathbf{T}^{\boldsymbol{T}}\left(\frac{\partial \mathbf{n}}{\partial r}\frac{\partial \mathbf{n}^T}{\partial r} + \frac{\partial \mathbf{n}}{\partial z}\frac{\partial \mathbf{n}^T}{\partial z}\right) - \left(Q - \rho c_p \frac{\partial \mathbf{T}^{\boldsymbol{T}}}{\partial \tau}\mathbf{n}\right)\mathbf{n}^{\boldsymbol{T}}\right] dV + \\ + \int_S (q\mathbf{n}^T + \alpha(\mathbf{T}^{\boldsymbol{T}}\mathbf{n} - T_0)\mathbf{n}^T) dS \tag{26}$$

The system (26) can be written in a matrix form analogous to equation (23):

$$\mathbf{HT} + \mathbf{C}\frac{\partial \mathbf{T}}{\partial \tau} + \mathbf{p} = \mathbf{0} \tag{27}$$

where $\mathbf{H}$ and $\mathbf{p}$ are matrices given by (24), and $\mathbf{C}$ can be expressed as:

$$\mathbf{C} = \int_V \rho c_p \mathbf{n}\,\mathbf{n}^T dV \tag{28}$$

An assumption of linear temperature change in very short time interval $\Delta\tau$ and application of weighted Galerkin's residual method leads to an equation which is a discrete (with respect to time) counterpart of equation (27).

$$\overline{\mathbf{H}}\mathbf{T}_{i+1} + \overline{\mathbf{p}} = \mathbf{0} \tag{29}$$

Matrix $\overline{\mathbf{H}}$ and vector $\overline{\mathbf{p}}$ in equation (29) are described by the following relations:

$$\overline{\mathbf{H}} = \left(2\mathbf{H} + \frac{3}{\Delta\tau}\mathbf{C}\right) \\ \overline{\mathbf{p}} = \left(\mathbf{H} - \frac{3}{\Delta\tau}\mathbf{C}\right)\boldsymbol{T}_i + 3\mathbf{p} \tag{30}$$

Equation (29) can be used to compute the vector of nodal temperatures $\mathbf{T}_{i+1}$ after a time step $\Delta\tau$ (i.e. at $\tau = \tau_{i+1} = \tau_i + \Delta\tau$) provided that initial value $\mathbf{T}_i$ for $\tau = \tau_i$ is known.

5. Mechanical model

A mathematical model of the compression process is based on the theory of plastic flow (Chakrabarty, 2006). The principle of the upper assessment (Bower, 2010), calculus of variations (Adhikari, 1998), approximation theory and optimization methods (Findaeisen at al., 1980 ; Nocedal & Wright 2006) and numerical methods for solving partial differential equations (Evans 1988; Polyanin, & Zaitsev, 2004; Pinchover & Rubinstein, 2005), including the finite element method (Zienkiewicz at al., 2005) were used. The following assumptions were established:

- deformation and stress state are axial-symmetrical,
- deformed material is isotropic but inhomogeneous,
- the material behaviour is rigid-plastic - the relationship between the stress tensor and strain rate tensor is calculated according to the Levy-Mises flow law, which is given as:

$$\sigma_{ij} - \frac{1}{3}\sigma_{kk}\delta_{ij} = \frac{2}{3}\frac{\sigma_p}{\dot{\varepsilon}_i}\dot{\varepsilon}_{ij} \tag{31}$$

Rigid-plastic model was selected due to its very good accuracy at the strain field during the hot deformation and sufficient correctness of calculated deviatoric part of the stress field. Moreover, the elastic part of each stress tensor component is very low at temperatures close to solidus line and can in practice be neglected in calculations of strain distribution. The limits for plastic metal behavior are defined according to Huber-Mises-Hencky yield criterion:

$$\sigma_{ij}\sigma_{ij} = 2\left(\frac{\sigma_p}{\sqrt{3}}\right)^2 \tag{32}$$

In equations (31) and (32) σ_{ij} denotes the stress tensor components, σ_{kk} represents the mean stress, δ_{ij} is the Kronecker delta, σ_p indicates the yield stress, $\dot{\varepsilon}_i$ is the effective strain rate, and $\dot{\varepsilon}_{ij}$ denotes strain rate tensor components. The components are given by an equation:

$$\dot{\varepsilon}_{ij} = \frac{1}{2}\left(\nabla_i v_j + \nabla_j v_i\right) \tag{33}$$

In cylindrical coordinate system $Or\theta z$ the solution is a vector velocity field defined by the distribution of three coordinates $\boldsymbol{v} = (v_r, v_\theta, v_z)$. The field is a result of optimization of a power functional, which can be written in general form as the sum of power necessary to run the main physical phenomena related to plastic deformation. Due to the axial-symmetry of the sample the velocity field the circumferential component of the velocity field can be neglected and the functional is usually formulated as:

$$J[\boldsymbol{v}] = \dot{W} = \dot{W}_\sigma + \dot{W}_\lambda + \dot{W}_f \tag{34}$$

Component $\dot{W}_\sigma$ occurring in equation (34) represents the plastic deformation power, $\dot{W}_\lambda$ is the power which is a penalty for the departure from mass conservation condition, $\dot{W}_f$ denotes the friction power and $\boldsymbol{v} = (v_r, v_z)$ describes the reduced velocity field distribution.

Rigid-plastic formulation of metal deformation problem requires the condition of mass conservation in the deformation zone. In case of solids and liquids with a constant density, this condition can be simplified to the incompressibility condition. Such a condition is generally satisfied with sufficient accuracy during the optimization of functional (34). In most solutions a slight, but noticeable loss of volume is observed. The loss is caused by incomplete fulfilment of the incompressibility condition imposed on the solution in numerical form. It is negligible in case of traditional computer simulation of deformation processes although in some embodiments more accurate methods are used to restore the volume of metal subjected to the deformation. Unlike this case the density of semi-solid materials varies during the deformation process and these changes result in a physically reasonable change in the volume of a body having constant mass. The size of the volume loss due to numerical errors is comparable with changes caused by fluctuation in the density of the material.

A further problem specific to the variable density continuum is power $\dot{W}_\lambda$, which occurs in functional (34). It is used in most solutions and has a significant share of total power. Even when the iterative process approaches the end, this power component is still significant, especially if the convergence of the optimization procedures is insufficient. In case of discretization of the deformation area (e.g. using the finite element method) if one focuses solely on the $\dot{W}_\lambda$ a number of possible optimal solutions appear. They are related to a number of possible directions of movement of discretization nodes providing the volume preservation of the deformation zone. Each of these solutions creates a local optimum for $\dot{W}_\lambda$ power and thus for the entire functional (34). This makes it difficult to optimize because of lack of uniform direction of fall of total power which leads to global optimum. The material density fluctuation causes further optimization difficulties, resulting from additional replacement of incompressibility condition with a full condition of mass conservation.

The proposed solution requires high accuracy in ensuring the incompressibility condition for the solid material or mass conservation condition for the semi-solid areas. This approach stems from the fact that the errors resulting from the breach of these conditions can be treated as a volume change caused by the steel density variation in the semi-solid zone. High accuracy solution is required also due to large differences in yield stress for the individual subareas of the deformation zone. In the discussed temperature range they appear due to even slight fluctuations in temperature. In presented solution the second component of functional (34) is left out and mass conservation condition is given in analytical form constraining the radial (v_r) and longitudinal (v_z) velocity field components. The functional takes the following shape:

$$J[\boldsymbol{v}] = \dot{W}_\sigma + \dot{W}_t \tag{35}$$

In case of functional (35) the numerical optimisation procedure converges faster than the one for functional (34) due to the reduced number of velocity field parameters (only radial components are optimisation parameters) and the lack of numerical form of mass conservation condition. The accuracy of the proposed hybrid solution is higher also due to negligible volume loss caused by numerical errors which is very important for materials with variable density.

As mentioned before the solution of the problem is a velocity field in cylindrical coordinate system in axial-symmetrical state of deformation. Optimization of metal flow velocity field in the deformation zone of semi-variational problem requires the formulation according to equation (35). The radial velocity distribution $v_r(r,\theta,z)$ and the longitudinal one $v_z(r,\theta,z)$ are so complex that such wording in the global coordinate system poses considerable difficulties. These difficulties are the result of the mutual dependence of these velocities. Therefore the basic formulation will be written for the local cylindrical coordinate system $Or\theta z$ with a view to the future discretization of deformation area using one of the dedicated methods. In addition one will find that the deformation of cylindrical samples is characterized by axial symmetry. As demonstrated by experimental studies conducted using semi-solid samples the symmetry may be disturbed only as a result of unexpected leakage of liquid phase.

Such experiments, however, are regarded as unsuccessful and not subject to numerical analysis. Establishment of the axial symmetry, which except in cases of physical instability can be considered valid also for the process of compression or tensile test of semi-solid

samples, allows one to simplify the model because of the identical strain distribution at any axial sample cross-section. Considerations will therefore be carried out in Orz coordinates for the sample cross-sectional using one of the planes containing the sample axis. Components of power functional given by (35) have been formulated in accordance with the general theory of plasticity by relevant equations. The plastic power for the deformation zone having volume of V is given by the subsequent relation:

$$\dot{W}_\sigma = \int_V \sigma_i \dot{\varepsilon}_i \, dV \tag{36}$$

where σ_i is the effective stress and $\dot{\varepsilon}_i$ denotes the effective strain. The plastic deformation starts when the rising effective stress reaches yield stress limit σ_p ($\sigma_i = \sigma_p$) according to yield criterion given by equation (32). Effective strain occurring in equation (36) is calculated on the basis of the strain tensor components $\dot{\varepsilon}_{ij}$ according to following relationship:

$$\dot{\varepsilon}_i = \sqrt{\frac{2}{3}\dot{\varepsilon}_{ij}\dot{\varepsilon}_{ij}} \tag{37}$$

The components are given by equation (33). For axial-symmetrical case the strain has a form:

$$\begin{pmatrix} \frac{\partial v_r}{\partial r} & 0 & \frac{1}{2}\frac{\partial v_r}{\partial z} + \frac{1}{2}\frac{\partial v_z}{\partial r} \\ 0 & \frac{v_r}{r} & 0 \\ \frac{1}{2}\frac{\partial v_r}{\partial z} + \frac{1}{2}\frac{\partial v_z}{\partial r} & 0 & \frac{\partial v_z}{\partial z} \end{pmatrix} \tag{38}$$

The second component of functional (35) is responding for friction. To compute friction power on the boundary S of area V a model given by the subsequent equation was used:

$$\dot{W}_t = \int_S m\frac{\sigma_p}{\sqrt{3}}\|\bar{\boldsymbol{v}}\| \, dS \tag{39}$$

In equation (39) m is the so called friction factor which is usually experimentally selected and $\bar{\boldsymbol{v}}$ is a relative velocity vector of metal and tool $\bar{\boldsymbol{v}} = \boldsymbol{v} - \boldsymbol{v_t}$. In case of tensile test the samples are permanently fixed in jaws of a physical simulator and friction must not be taken into account. However, compression test requires sharing the friction power which is significant.

5.1 The model of sample velocity field

Clearly defined deformation field resulting from the optimal solution of functional (37) cannot be calculated without one of the conditions mentioned before. For the solid zones the incompressibility condition can be described by universal operator equation independently of the mechanical state of the deformation process:

$$\nabla \boldsymbol{v} = 0 \tag{40}$$

Because the semi-solid zone is characterized by density change due to still ongoing progress of steel state of aggregation, the condition of incompressibility is inadequate to reflect changes and was replaced with the mass conservation condition, which describes the following modified operational equation:

$$\nabla \boldsymbol{v} - \frac{1}{\rho}\frac{\partial \rho}{\partial t} = 0 \tag{41}$$

The basis for the optimization of functional (35) is the velocity field determined by appropriate system of velocity functions in the concerned area. These functions are then the source of deformation field and other physical quantities affecting the power functional formulation. Obtaining an accurate real velocity field requires the use of velocity functions depending on a number of variational parameters. The functions should be flexible enough to map the field throughout the whole volume of the deformation zone. Analytical description of each component of the velocity field with a single function in the whole area of deformation is not preferred. This approach creates difficulties especially in areas not subjected to the deformation where the velocity function should remain constant. Therefore, the solution to the problem of semi-solid metal flow was based on the method proposed by Malinowski in (Malinowski, 1986, 1997, 2005). This method involves the breakdown of the elements and the deformation velocity field approximation by polynomials with coefficients different for each element. The method was originally applied to solutions with a constant volume. The author of the current paper has developed a new method for semi-solid materials by adapting the source one to the analysis of materials with variable density.

In the case of deformation of axial-symmetrical bodies the incompressibility condition is given by following differential equation:

$$\frac{\partial v_r}{\partial r} + \frac{v_r}{r} + \frac{\partial v_z}{\partial z} = 0 \tag{42}$$

For the semi-solid area equation (42) is replaced by the mass conservation condition due to existing density changes. The longitudinal velocity has been calculated as an analytical function of radial velocity using this condition. In cylindrical coordinate system the condition has been described with an equation:

$$\frac{\partial v_r}{\partial r} + \frac{v_r}{r} + \frac{\partial v_z}{\partial z} - \frac{1}{\rho}\frac{\partial \rho}{\partial \tau} = 0 \tag{43}$$

Equation (42) is a special case of equation (43) and therefore the proposed solution will consider the dependence (43) as more general. In (43) ρ is the temporary material density and τ is the time variable. The proposed variational formulation makes the longitudinal velocity dependent on the radial one. Condition (43) allows for the calculation of $\partial v_z/\partial z$ derivative as a function of $\partial v_r/\partial r$ after analytical differentiation of radial velocity distribution function $v_r(r,z)$. Hence, the longitudinal velocity is calculated as a result of analytical integration according to following equation:

$$v_z = -\int \left(\frac{\partial v_r}{\partial r} + \frac{v_r}{r} - \frac{1}{\rho}\frac{\partial \rho}{\partial \tau} \right) dz \tag{44}$$

In this case the velocity field depends only on one function – the radial velocity distribution. Both the components (v_r and v_z) satisfy the mass conservation imposed on the velocity field. The functional takes the form of equation (35) and in case of application of one of the methods requiring discretization (FEM, FDM or any meshless method) the number of discrete parameters is significantly reduced (at least by half). Only the right class of the velocity field distribution functions is problematic. The functions must be relevant for description of the material deformation and sufficiently flexible. Hence, the whole control volume is usually divided into sub-areas and the functions are defined in local coordinate systems for each sub-region. It requires the definition of both the local system and transformation from local to global one. The r coordinate acts as an independent variable (abscissa) in global area and varies in the range of r_m to R_m. The z coordinate depends on r and is limited by functions describing both the area boundaries: lower $z_l = f(r)$ and upper $z_u = g(r)$. Considering all the assumptions two linear functions, binding both the systems - global Orz and local one $O\xi\eta$ were defined

$$\begin{aligned} \xi(r,z) &= \frac{r}{R_m} \\ \eta(r,z) &= \frac{2z - g(r) - f(r)}{g(r) - f(r)} \end{aligned} \tag{45}$$

The main assumption of the presented model is the dependence of the longitudinal velocity distribution function $v_z(\xi,\eta)$ on the radial velocity distribution function $v_r(\xi,\eta)$. For this purpose, the form of the function v_r has to be determined on the basis of analysis of the velocity field components distribution in the control area. For further discussion one assumes the following form v_r function:

$$v_r(\xi,\eta) = \frac{1}{2}\frac{r v_0}{g(r) - f(r)}\left(1 + \frac{\partial \psi(\xi,\eta)}{\partial \eta}\right) \tag{46}$$

where v_0 is the GLEEBLE jaw velocity and $\psi(\xi,\eta)$ is a distribution function of velocity field components in local coordinate system. It should be remembered that for the areas in which the steel is in solid state the incompressibility condition given by dependence (42) should be taken into account and for zones with semi-liquid steel mass conservation equation (43) is valid. Linking the longitudinal velocity v_z with the radial one is done precisely through these two conditions. Taking into account the more general equation (43) and assuming a known value of the radial velocity one can be determine the longitudinal one using the following dependence:

$$v_z(\xi,\eta) = \int \left[\frac{1}{\rho}\frac{\partial \rho}{\partial t} - \frac{\partial v_r(\xi,\eta)}{\partial r} - \frac{v_r(\xi,\eta)}{r} \right] dz \tag{47}$$

The consequence of such a conduct is the fact that this condition is imposed on the velocity field in an analytical form. As already mentioned it is of major importance for optimizing the correct flow field for the steel being in semi-solid conditions.

In order to relate both the velocities the derivative of the velocity with respect to the radial coordinate has to be calculated first. Having in mind the dependence of f and g on r and similar one of ψ on ξ and on η one can write:

$$\frac{\partial v_r}{\partial r} = \frac{v_0}{2}\left[\frac{\partial}{\partial r}\left(\frac{r}{g-f}\right)\left(1+\frac{\partial \psi}{\partial \eta}\right)+\frac{r}{g-f}\frac{\partial}{\partial r}\left(1+\frac{\partial \psi}{\partial \eta}\right)\right] \tag{48}$$

After some differentiations and arrangements relationship (48) can be written in a form:

$$\frac{\partial v_r}{\partial r} = \frac{v_0}{2(g-f)}\left(1+\frac{\partial \psi}{\partial \eta}+\xi\frac{\partial^2 \psi}{\partial \xi\,\partial \eta}\right)-\frac{r v_0\left(\frac{\partial g}{\partial r}-\frac{\partial f}{\partial r}\right)}{2(g-f)^2}\left[1+\frac{\partial \psi}{\partial \eta}+\frac{\partial^2 \psi}{\partial \eta^2}\left(\frac{\frac{\partial g}{\partial r}+\frac{\partial f}{\partial r}}{\frac{\partial g}{\partial r}-\frac{\partial f}{\partial r}}+\eta\right)\right] \tag{49}$$

Taking into account equation (49) and relationship (43) one can calculate the derivative of the longitudinal velocity with respect to z.

$$\begin{aligned}\frac{\partial v_z}{\partial z} = -\frac{\partial v_r}{\partial r}-\frac{v_r}{r}+\frac{1}{\rho}\frac{\partial \rho}{\partial \tau} = \frac{r v_0\left(\frac{\partial g}{\partial r}-\frac{\partial f}{\partial r}\right)}{2(g-f)^2}\left[1+\frac{\partial \psi}{\partial \eta}+\frac{\partial^2 \psi}{\partial \eta^2}\left(\frac{\frac{\partial g}{\partial r}+\frac{\partial f}{\partial r}}{\frac{\partial g}{\partial r}-\frac{\partial f}{\partial r}}+\eta\right)\right]- \\ -\frac{v_0}{2(g-f)}\left(1+\frac{\partial \psi}{\partial \eta}+\frac{1}{2}\xi\frac{\partial^2 \psi}{\partial \xi\,\partial \eta}\right)+\frac{1}{\rho}\frac{\partial \rho}{\partial \tau}\end{aligned} \tag{50}$$

After appropriate integration the velocity is given by the following relationship:

$$\begin{aligned}v = -\frac{v_0}{4}\left\{2\left(\eta+\frac{g+f}{g-f}+\psi\right)+\xi\frac{\partial \psi}{\partial \xi}-\frac{\left(\frac{\partial g}{\partial r}-\frac{\partial f}{\partial r}\right)}{g-f}\left[\eta+(1-r)\psi+r\left(\frac{\frac{\partial g}{\partial r}+\frac{\partial f}{\partial r}}{\frac{\partial g}{\partial r}-\frac{\partial f}{\partial r}}+\eta\right)\frac{\partial \psi}{\partial \eta}\right]\right\}+ \\ +\frac{\eta(g-f)+g+f}{2\rho}\frac{\partial \rho}{\partial \tau}\end{aligned} \tag{51}$$

Function $\psi = \psi(\xi,\eta)$ occurring in all the relationships describing the velocity field can be under the Weierstrass theorem approximated by polynomials. Approximation of $\psi(\xi,\eta)$ with the help of one polynomial in the whole deformation zone, although possible in some cases, is impractical and is a source of many problems. On the other hand the division of areas into smaller sub-areas requires continuity. To ensure continuity of the velocity field

and strain field in the whole zone of deformation, including the boundaries of the sub-regions, function $\psi(\xi,\eta)$ should be at least of class C^2.

6. Density changes and their influence on remaining models

In the proposed solution one of the most important parameters is the density. Its changes influence the mechanical part of the presented model and strongly depend on the temperature. The knowledge of effective density distribution is very important for modelling deformation of mushy materials. In the presented solution a model of density changes based on empirical data was applied.

Density distribution is one of the most important properties of the mushy steel which is subjected to the deformation. Its changes have influence on both the mechanical and thermal parts of the presented model. On the other hand, the density is strongly dependent on the temperature. Moreover, the solidification process causes non-uniform density distribution in the controlled volume. Since, the knowledge concerning effective density distribution is very important for the behaviour of deformation of porous and mushy materials and the modelling of such species requires good density changes model.

Density variations of liquid, semi-solid and solid materials are ruled by three phenomena:

- solid phase formation,
- laminar liquid flow through porous material and
- thermal shrinkage.

Transient rate of density changes is ruled by an equation:

$$\frac{\partial \rho}{\partial \tau} = \frac{\partial \rho_p}{\partial \tau} + \frac{\partial \rho_f}{\partial \tau} + \frac{\partial \rho_t}{\partial \tau} \tag{52}$$

In (52) the subsequent right hand derivatives of ρ_p, ρ_f i ρ_t with respect to transient time variable τ denote the density changes as a result of three mentioned phenomena One may calculate the density changes due to solid phase formation according to the relationship:

$$\frac{\partial \rho_p}{\partial \tau} = [\rho_s(1 - X_l) + \rho_l X_l]\left(\frac{\rho_s}{\rho_l} - 1\right)\frac{\partial X_l}{\partial \tau} \tag{53}$$

where X_l and X_s are the shares of liquid and solid phases are semi-steel. Changes in density caused by laminar flow of the liquid phase through the porous material are described by the equation:

$$\frac{\partial \rho_f}{\partial \tau} = \rho_l X_l \left(\frac{\partial v_r}{\partial r} + \frac{v_r}{r} + \frac{\partial v_z}{\partial z}\right) \tag{54}$$

In (54) v is the velocity of the metal particles flow. Changes in density due to thermal shrinkage depend on the speed of changes in temperature and coefficients of linear thermal expansion β_s i β_l of both solid and liquid phases:

$$\frac{\partial \rho_t}{\partial \tau} = [\beta_s \rho_s (1 - X_l) + \beta_l \rho_l X_l] \frac{\partial T}{\partial \tau} \tag{55}$$

where T is the temperature on an absolute scale. Issues of density changes mechanisms were the subject of (Glowacki, 2002). Changes in the density as a result of the velocity and temperature of the metal particles substantially complicate the problem of optimizing the metal flow velocity field. Coupled solution of all the problems is difficult and very often an uncoupled model is used.

6.1 Empirical model of density changes

The density changes model is rather complex and its solution is associated with an additional increase in computational complexity of the total solution. Regardless of the solution used the development of a right model is a problem in itself. It requires addressing a number of issues related to the change of state, the flow of the liquid phase in the presence of solid steel frames, etc. This is an important issue - however, it requires commitment of substantial computer resources and long computation times. Hence another way of taking density into consideration is possible due to temperature dependency of this quantity (Glowacki, 1996). In order to avoid additional problems with solution of differential equation, density changes were calculated according to an empirical model taking into consideration experimental data. The model is slightly less accurate but such a method makes the solution much easier. The solution seems to be a good alternative way to predict changes in mushy steel. In proposed approach the density is depending on:

- temperature,
- chemical composition of the material and,
- steel microstructure.

The study published in (Glowacki, 1998), which is result of investigation carried out for steel in the solid state, shows that for typical forming processes impact of a steel grade on change in the density resulting from temperature changes is small. For determination of density in these conditions for both carbon and low-alloy steels it is proposed to apply following empirical equation:

$$\rho = \frac{7850}{(1 + \Delta l)^3}; \left[\frac{\mathrm{kg}}{\mathrm{m}^3}\right] \tag{56}$$

In equation (56) Δl is calculated according to following formula:

$$\Delta l = 0{,}004 \left(\frac{T + 273}{1000}\right)^2$$

Similar equation can be used for austenitic steels:

$$\rho = \frac{7897}{(1 + \Delta l)^3}; \left[\frac{\mathrm{kg}}{\mathrm{m}^3}\right] \tag{57}$$

The Δl parameter from (57) is calculated as:

$$\Delta l = -0{,}00358 + 0{,}00947\frac{T+273}{1000} + 0{,}0103\left(\frac{T+273}{1000}\right)^2 - 0{,}00298\left(\frac{T+273}{1000}\right)^3$$

Similar dependence can be used for high-alloy steels. In this case it is necessary to modify the equation (56) in a manner appropriate for the particular steel grade. Thus, for temperature range which is proper for traditional process of steel hot deformation the calculation of changes in density seems to be pretty simple. Such temperatures are characteristic for certain sample areas.

Otherwise presents itself the problem for higher temperature ranges, where the deformation occurs during the simultaneous metal solidification. Here the density variations may be significant. For purposes of the current mathematical model an approach proposed by Mizukami was used (Mizukami at al., 2002). For carbon steels containing no other elements the density changes are functions of temperature. Steels were tested with a wide range of carbon content, which ranges from 0.005% to 0.56% by mass. The authors develop tests for typical steels having chemical composition expressed in% by mass given in Table. 1.

Left side of Figure 1 shows the change in density for MC1 grade steel as a function of temperature. For steel changing its states of aggregation some plots of density in the various phases of the transformation process has been developed. The right side of Figure 1 shows the course of the changes in the density of liquid phase as a function of ΔT_l – undercooling temperature with respect to the liquidus line. Changes in density are presented in relation to the base density of 7060 [kg/m^3].

Steel	ULC	LC	MC1	MC2	HC
[C]	0.005	0.040	0.110	0.140	0.550
[Si]	0.010	0.040	0.100	0.160	0.150
[Mn]	0.120	0.190	0.480	0.540	0.910
[P]	0.014	0.026	0.020	0.016	0.021
[S]	0.003	0.006	0.008	0.003	0.001

Table 1. Chemical composition (mass %) of typical steels tested by authors of (Mizukami at al., 2002).

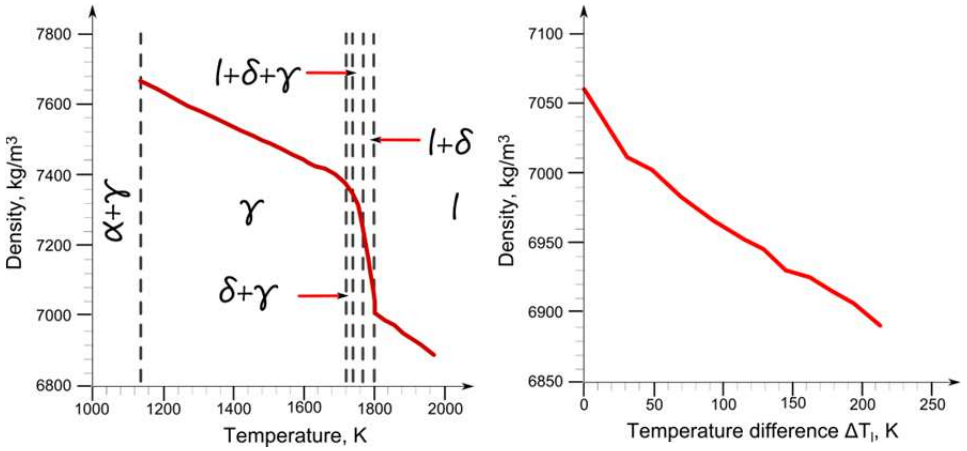

Fig. 1. Density of MC1 grade steel as a function of temperature (left) and density changes of its liquid phase as a function of temperature increase (right). Plots are based on data published in (Mizukami at al., 2002).

Subsequent charts presented in Figure 2 show changes in density of δ i γ phases, respectively. Both of them are functions of undercooling temperature ΔT_δ and ΔT_γ of appropriate phases with respect to solidus temperature.

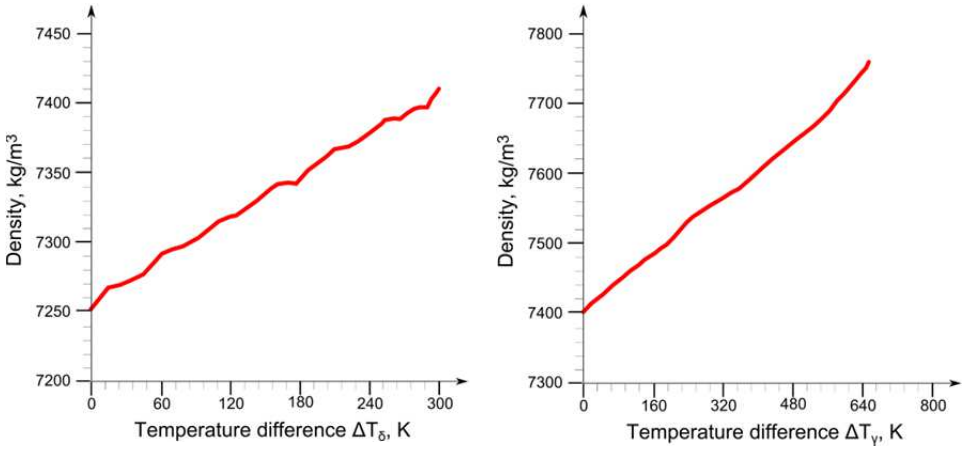

Fig. 2. Density changes of steel phase δ (left) and γ (right) of MC1 steel grade as a function of temperature increase – based on data published in (Mizukami at al., 2002).

The presented graphs were used to develop analytical dependencies, which describe changes in the density of steel during the transformation of state of aggregation. In the region of coexistence of δ and γ phases density was estimated using the additivity rule. The correctness of this approximation was verified by comparing the theoretical results with those which were obtained from the measured values.

The density of carbon steels depends on the temperature and the existing fraction of liquid phase. The effect of alloying elements (except of coal) on the density of each steel phase is small, although the concentration of these components significantly affect the fraction of the phases. The density of each phase is calculated according to the following equations:

$$\begin{aligned} \rho_l &= 7{,}02 - 5{,}50 \cdot 10^{-4}\, \Delta T_l \\ \rho_\delta &= 7{,}27 + 3{,}07 \cdot 10^{-4}\, \Delta T_\delta \\ \rho_\gamma &= 7{,}41 + 4{,}80 \cdot 10^{-4}\, \Delta T_\gamma \end{aligned} \tag{58}$$

In equation (58) ρ_l, ρ_δ and ρ_γ indicate densities of liquid steel and its δ and γ phases, respectively. The density in the regions of occurrence of several phases simultaneously is given by the following equations:

$$\begin{aligned} \rho_{l+\delta} &= \rho_l^0 + \Delta\rho_{l/\delta} \cdot X_\delta \\ \rho_{l+\gamma} &= \rho_l^0 + \Delta\rho_{l/\gamma} \cdot X_\gamma \\ \rho_{l+\delta+\gamma} &= \rho_l^0 + \rho_{l/\delta} \cdot f_\delta + \Delta\rho_{l/\gamma} \cdot f_\gamma \end{aligned} \tag{59}$$

where ρ_l^0 denotes the density of the liquid phase for temperature discrepancy ΔT_l, $\Delta\rho_{l/\delta}$ and $\Delta\rho_{l/\gamma}$ are density differences between δ and γ phases for temperature drop from liquidus to solidus level, X_δ and X_γ are the fractions of δ i γ phases in surrounding liquid phase, respectively. and finally f_δ i f_γ are relative fractions of δ i γ phases. The density of $\delta + \gamma$ phase was estimated according to relationship:

$$\rho_{\delta+\gamma} = \rho_\delta \cdot X_\delta + \rho_\gamma \cdot X_\gamma \tag{60}$$

7. Mushy steel flow stress curves development

The subsequent part of the chapter deals with the computation of mushy steel flow stress curves based on the developed mathematical model which helps to avoid interpretational problems occurring in traditional testing procedures. Proper interpretation of the experimental results is possible with the help of appropriate computer aided testing system. Such a user friendly dedicated computer system with variable density has been developed (Glowacki & Hojny, 2009; Hojny & Glowacki, 2009a). The system codename called *Def_Semi_Solid* is a result of theoretical research conducted in a team lead by the chapter author with the financial support of grants awarded by Polish Committee of Scientific Research. The system in itself is not a subject of the chapter and its details are not discussed. The program was developed using an object oriented technique and is compatible with both Windows and Unix based platforms.

During experiments a few quantities were recorded. Among them the most important are GLEEBLE jaws displacement, force and temperature. This is a start point for the inverse analysis. The system calculates the shape and size of the deformation zone and strain and stress fields as well as optimal values of flow stress curve parameters. The model described in the previous section allows for the comparison of theoretical and experimental results for non-uniform temperature field. Isothermal tests in the temperature range over 1400 °C are impossible even using sophisticated equipment like GLEEBLE simulator. The presented model is a solution to the experimental problems. The

analysis of metal flow in subsequent regions of the sample deformation zone requires adequate methods. Classical techniques of interpretation of results of compression testing procedures fail due to significant samples barrelling which is inevitable at any temperature close to solidus level and which requires right analysis of metal flow in subsequent regions of the sample deformation zone.

A number of steel grades were subjected to series of experiments in Institute for Ferrous Metallurgy in Gliwice, Poland using GLEEBLE 3800 simulator. Example results of examination of two steels are reported in the current contribution. The first one is the 18G2A grade steel having 0.16% of carbon and the second was the S355J2G3So grade with 0.11% of carbon content. The essential aim of the investigation was the reconstruction of both temperature changes and strain evolution on specimen exposed to simultaneous deformation and solidification. The inverse procedure has been reported in (Glowacki & Hojny, 2009). Example results of inverse analysis are shortly described in succeeding subsections.

7.1 Characteristic temperature levels

As mentioned before, apart from the liquidus and solidus temperatures, four other temperature levels are characteristic for the mushy steel behaviour. All the levels split the liquidus-solidus range into intervals. The most important for the extra high temperature rolling process design is the nil ductility temperature (NDT). The plastic deformation of a steel specimen is possible only below the NDT temperature. The temperature levels have to be calculated according to results of series of difficult experiments which are not a subject of the current paper. For carbon steels with the carbon content of around 0.1 % the equilibrium liquidus and solidus temperature levels are 1523°C and 1482°C, respectively and the NDT is 1420°C. One must note that the last one is a conventional temperature of a sample surface (indicated during experimental procedure). The maximum and minimum temperatures in the sample's central cross-section may differ by 60- 70 °C. The equilibrium liquidus and solidus temperatures for 18G2A grade steel are 1513°C and 1465°C, respectively. The measured mean value of NDT temperature of the steel falls into the range of 1420°C÷1425°C. The NDT is related to the temperature at which the last liquid phase particles existing in the central part of the sample disappear in static processes. It has been observed that for temperatures higher than NDT a remainder of liquid phase still exist in the central part of the sample (Hojny & Glowacki, 2009a). For dynamic cooling and deformation processes in some regions of the sample the remainder of liquid phase can be observed at temperatures lower than NDT because the difference between sample surface and its central region is higher than for quasi-static processes.

7.2 Yield stress functions

The well-known Voce formula (Voce, 1955) was adopted for the description of the shape of yield stress function. Figure 3 presents four subsequent stages of an example compression test at higher sample surface temperature, i.e. 1425°C for the quasi-static process. One can observe that the experiment was successful (no metal outflow) and the deformation of the sample was realised despite the significant barrelling of the sample.

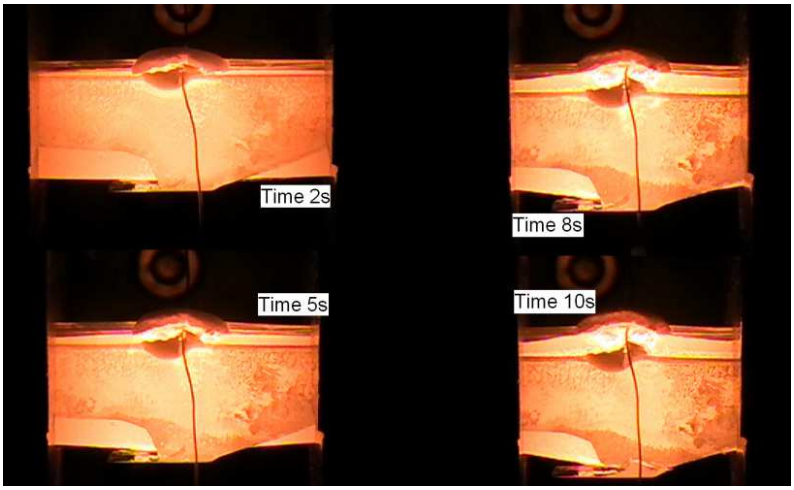

Fig. 3. Four stages of the deformation process ran at temperature 1425°C for the quasi–static deformation process. The figure presents the central part of the sample.

Due to significant strain inhomogeneity inverse analysis is the only method allowing for appropriate calculation of coefficients of yield stress functions at any temperature higher than NDT. The objective function of the analysis was defined as a norm of discrepancies between calculated (F^c) and measured (F^m) loads in a number of subsequent stages of the compression according to the following equation:

$$\varphi(x) = \sum_{i=1}^{n} (F_i^c - F_i^m)^2 \tag{61}$$

where n is the number of subsequent intervals of stress versus strain curve. The theoretical forces F^c were calculated with the help of sophisticated numerical solver being the implementation of the model which was described in this chapter. Due to the very low level of recorded stresses the experimental curves obtained from the GLEEBLE machine are noisy. Before the application of inverse analysis they were smoothed using Fast Fourier Transformation (FFT) algorithm.

The final shape of the curves for 18G2A and S355J2G3So grade steels after interpretation using inverse analysis are presented in figures 8 and 16, respectively. Figure 4 summarise the results of calculation of example coefficients of Voce formula for 18G2A grade steel which was deformed in a quasi-static process. The effective strain inside the deformation zone varied from 0 to 0.6 and the effective strain rate reached its maximum value of 2.9 s^{-1} in final stage of the deformation process. The presented curves are plotted using the calculated coefficients of Voce curve for temperature levels observed in the sam ples' cross-sections and for strain rate equal to 1 s^{-1}.

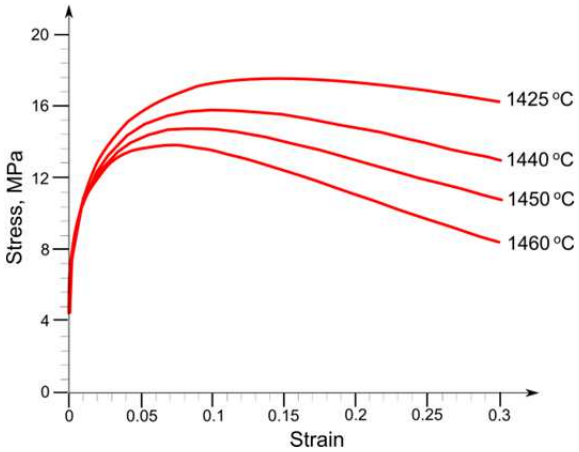

Fig. 4. Flow stress vs. strain at several temperature levels for 18G2A steel grade deformed during quasi-static process – strain rate 1 s-1 (Glowacki & Hojny, 2010).

Example results of investigation of S355J2G3So grade steel are presented in Figure 5. The investigation procedures were analogous to those applied in case of18G2A grade steel.

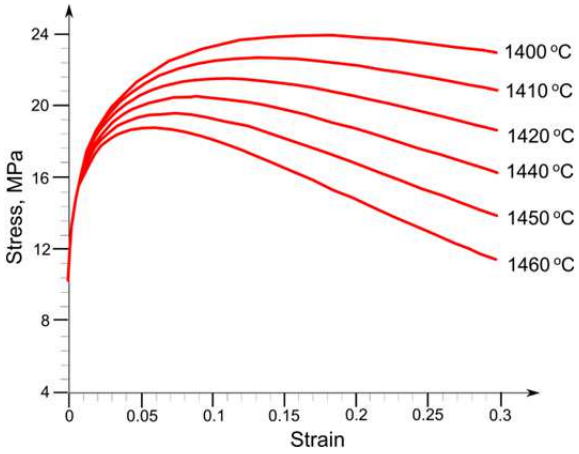

Fig. 5. Stress-strain curves at several temperature levels from the range of 1400-1450°C (S355J2G3So grade steel, quasi-static process – strain rate 1 s-1 (Glowacki & Hojny, 2010).

8. Conclusions

Modelling of deformation of steel samples with mushy zone requires resolving several problems which are characteristic for the temperature range close to the solidus level. Some of the problems are independent of the strain and stress state of the material and are similar for both axial-symmetrical and three dimensional cases. The computation of characteristic temperatures and temperature-dependent sudden changes of steel plastic properties require advanced methods of computer simulation. The most important property for material

plastic behaviour is the yield stress function describing strain-stress curve. The proposed analytical model allows computation of such kind relationships.

The chapter has been dedicated to hybrid numerical-analytical model of semi-solid steel behaviour under plastic deformation. Application of inverse analysis and the proposed model allows for the testing of rheological properties of steels at temperature higher than 1400 °C. The results of the research are crucial for a unique computer system allowing for proper interpretation of the results of very high temperature compression tests. The classical interpretation of such results is improper due to strong strain inhomogeneity. The developed system is a tool to overcome many interpretational problems allowing for the computation of the appropriate shape and parameters of yield-stress curves. The curves have crucial influence on the results of computer simulation of semi-solid steel deformation.

The model presented in the current contribution is an axial-symmetrical one. The author have run further investigations leading to the development of a fully three-dimensional model of integrated casting and rolling processes as well as the soft reduction process, that is a part of strip casting technology. Like the model presented in the hereby chapter the spatial one also focuses on three main aspects: thermal, mechanical and density changes. Further intention of the research is the development of fully three dimensional model of mushy steel behaviour during rolling of plates with mushy region. The model will be useful for technologists working on the development of an integrated casting and rolling process. It is the most recent technology of sheet steel production, which is very profitable and requires extremely low energy consumption – very important for steel and automotive industries.

The compression tests carried out have shown good predictive ability of the proposed solution. They show that the flow stress above the NDT is strongly temperature and strain rate dependent. Low carbon steels, having carbon content of 0.11% and 0.16%, have been investigated in wide temperature range and strain rate. Example results of the experimental work were presented delivering a set of equations describing rheological behaviour of the investigated steels. The presented model and experimental procedure requires further investigation leading to the improvement of the solution and modelling additional phenomena accompanying the simultaneous deformation and solidification processes.

9. Acknowledgments

The work has been supported by the Polish Ministry of Science and Higher Education - Grant No. N N508 585539.

10. References

Adhikari S.K. (1998). Variational principles for the numerical solution of scattering problems. Wiley, New York USA, ISBN 0471181935

Bower, A.F. (2010) Applied mechanics and solids, CRC Press – Taylor & Francis Group, New York USA, ISBN 987-1-4398-0247-2

Chakrabarty, J. (2006). Theory of plasticity. Elsevier Butterworth-Heinemann, Oxford UK, ISBN 978-0-7506-6638-2

Evans, L.C. (1998), Partial Differential Equations, American Mathematical Society, ISBN 0821807722.

Findaeisen, W., Szymanowski, J., Wierzbicki, A (1980). Theory and optimization methods. PWN, Warszawa, ISBN 8301009764

Glowacki, M. (1996). Finite element three-dimensional modelling of the solidification of a metal forming charge, *Journal of Materials Processing Technology*, Vol. 60, No. 1-4, pp. 501-504, ISSN 0924-0136

Glowacki, M. (1998). Thermal-mechanical–microstruktural model of shape rolling. *Dissertations and Monographs*, Vol. 76, AGH Publishing, Krakow Poland, ISSN 0867-6631

Głowacki, M. (2002) Possibilities of mathematical modeling of deformation of samples with mushy zone, *Proceedings of 44th Mechanical Working and Steel Processing Conference*, pp. 1151-1162, Orlando USA, September 1, 2002, ISBN 978-1-886362-62-8

Glowacki, M. (2006). Mathematical modelling of deformation of steel samples with mushy zone, In: *Research in Polish metallurgy at the beginning of XXI century, Committee of Metallurgy of the Polish Academy of Science*, K. Swiatkowski, (Ed.), 305-324, Publishing House Akapit, Krakow Poland

Glowacki, M. & Hojny, M. (2006). Development of a computer system for high temperature steel deformation testing procedure, *Proceedings of Simulation, Design and Control of Foundry Processes*, pp. 145-156, Krakow Poland, November 22-24, 2006

Glowacki, M. & Hojny, M. (2009). Inverse analysis applied for determination of strain-stress curves for steel deformed in semi-solid state, *Inverse Problems in Science and Engineering*, Vol.17, No. 2, pp. 159–174, ISSN 1741-5977

Glowacki, M. & Hojny, M. (2010). Investigation of mushy steel rheological properties at temperatures close to solidus level, In: *Polish metallurgy 2006–2010 in time of the worldwide economic crisis , Committee of Metallurgy of the Polish Academy of Science*, K. Swiatkowski, (Ed.), 193-212, Publishing House Akapit, Krakow, Poland, ISBN 978-83-60958-59-9

Glowacki, M., Hojny, M. & Jędrzejczyk, D. (2010). Hybrid analytical-numerical system of mushy steel deformation. In : *Recent studeis in meshless & other novel computational methods*, B. Sarler & S.N. Atluri, (Eds.), pp. 35-54, Tech Science Press, ISBN-10 0-9824205-4-4, USA

Hojny, M. & Glowacki, M. (2008). Computer modelling of deformation of steel samples with mushy zone, *Steel Research International*, vol. 79, No. 11, (2008), pp. 868-874, ISSN 1611-3683

Hojny, M. & Glowacki, M. (2009a) The methodology of strain – stress curves determination for steel in semi-solid state, *Archives of Metallurgy and Materials*, Vol. 54, No. 2, pp. 475–483, ISSN 1733-3490

Hojny, M. & Glowacki, (2009b) The physical and computer modelling of plastic deformation of low carbon steel in semi-solid state, *Transactions of the ASME, Journal of Engineering Materials and Technology*, Vol. 131 No. 4, pp. 041003-1–041003-7, ISSN 0094-4289

Hojny, M., Glowacki, M. & Malinowski Z. (2009), Computer aided methodology of strain-stress curve construction for steels deformed at extra high temperature, *High Temperature Materials and Processes*, Vol. 28, No. 4, pp. 245–252, ISSN 0334-6455

Hojny, M. & Glowacki, M. (2011). Modeling of Strain-Stress Relationship for Carbon Steel Deformed at Temperature Exceeding Hot Rolling Range, *Transactions of the ASME, Journal of Engineering Materials and Technology*, Vol. 133, No. 2, pp. 021008-1–021008-7, ISSN 0094-4289

Kang, C.G. & Yoon, J.H. (1997). A finite-element analysis on the upsetting process of semi-solid aluminum material, *Journal of Materials Processing Technology*, Vol. 66, No. 1-3, pp. 76-84, ISSN 0924-0136

Koc, M., Vazquez, V., Witulski, T. & Altan, T. (1996). Application of the finite element method to predict material flow and defects in the semi-solid forging of A356 aluminum alloys, *Journal of Materials Processing Technology*, Vol. 59, No. 4, pp. 106-112, ISSN 0924-0136

Kopp, R., Choi, J. & Neudenberger D. (2003). Simple compression test and simulation of an Sn–15% Pb alloy in the semi-solid state, *Journal of Materials Processing Technology*, Vol. 135, No. 2-3, pp. 317-323, ISSN 0924-0136

Leader, J. J. (2004). Numerical Analysis and Scientific Computation. Addison Wesley, Boston Massachusetts, ISBN 978-0-201-73499-7

Li, J.Y., Sugiyama, S. & Yanagimoto, J. (2005), Microstructural evolution and flow stress of semi-solid type 304 stainless steel, *Journal of Materials Processing Technology*, Vol. 161, No. 3, pp. 396-406, ISSN 0924-0136

Malinowski, Z. (1986). Analysis of upsetting process based on velocity fields, PhD thesis, AGH Krakow Poland, in Polish

Malinowski, Z. (1997). Effect of heat generation on flow stress deformation based on the axially symmetric compression test. Metallurgy & Foundry Engineering, 23, 1997, 459-467, ISSN 1239-2325

Malinowski Z. (2005). Numerical models in metal forming and heat transfer. Wyd. AGH Publishing, Krakow Poland, in Polish, ISBN: 83-89388-98-7

Mizukami, H., Yamanaka, A. & Watanabe, T. (2002). Prediction of density of carbon steels, *ISIJ International*, Vol. 42, No. 4, pp. 375-384, ISSN 0915-1559

Nocedal J. & Wright S.J. (2006). Numerical Optimization. Springer-Verlag, Berlin Germany. ISBN 0-387-30303-0

Pinchover, Y. & Rubinstein, J. (2005). An Introduction to Partial Differential Equations, New York: Cambridge University Press, ISBN 0521848865.

Polyanin, A.D. & Zaitsev, V.F. (2004). Handbook of Nonlinear Partial Differential Equations, Boca Raton: Chapman & Hall/CRC Press, ISBN 1584883553.

Sang-Yong, L., Jung-Hwan L. & Young-Seon L. (2001). Characterization of Al 7075 alloys after cold working and heating in the semi-solid temperature range. *Journal of Materials Processing Technology*, Vol. 111, No. 1-3, pp. 42-47, ISSN 0924-0136

Seol, D.J., Won, Y.M., Yeo, T., Oh, K.H., Park, J.K. & Yim, C.H. (1999). High Temperature Deformation Behavior of Carbon Steel in the Austenite and δ-Ferrite Regions, *ISIJ International*, Vol. 39, No. 1, pp. 91-98, ISSN 0915-1559

Seol, D.J., Oh, K.H., Cho, J.W., Lee, J.E., Yoon, U.S. (2002). Phase-field modelling of the thermo-mechanical properties of carbon steels, Acta Materialia, Vol. 50, No. 9, pp. 2259-2268, ISSN 1359-6454

Senk, D., Hagemann, F., Hammer, B., Kopp, R., Schmitz, H.P. & Schmitz, W. (2000). Umformen und Kühlen von direktgegossenem, Stahlband, *Stahl und Eisen*, Vol. 120, No. 6, pp. 65-69, ISSN 0340-4803

Suzuki, H.G., Nishimura, S. & Yamaguchi S. (1988). Physical simulation of the continuous casting of steels, *Proceedings of Physical Simulation of Welding, Hot Forming and Con- tinuous Casting*, pp. 166-191, Canmet Canada, May 2-4, 1988

Voce, E. (1955). A Practical Strain Hardening Function, *Metallurgia*, vol. 51, 1955, pp. 219-226, ISSN 0141-8602

Zhao Y.Q., Wu W.L. & Chang H. (2006). Research on microstructure and mechanical properties of a new α + Ti2Cu alloy after semi-solid deformation, *Materials Science and Engineering*, Vol. 416, No. 1-2, pp. 181-186, ISSN 0921-5093

Zienkiewicz, O.C., Taylor, R. L. & Zhu, J.Z. (2005). The Finite Element Method: Its Basis and Fundamentals, Elsevier Butterworth-Heinemann, Oxford UK, ISBN 0-7506-6320-0

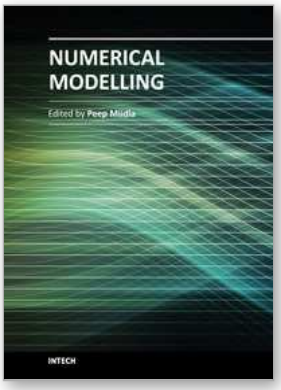

Numerical Modelling

Edited by Dr. Peep Miidla

ISBN 978-953-51-0219-9
Hard cover, 398 pages
Publisher InTech
Published online 23, March, 2012
Published in print edition March, 2012

This book demonstrates applications and case studies performed by experts for professionals and students in the field of technology, engineering, materials, decision making management and other industries in which mathematical modelling plays a role. Each chapter discusses an example and these are ranging from well-known standards to novelty applications. Models are developed and analysed in details, authors carefully consider the procedure for constructing a mathematical replacement of phenomenon under consideration. For most of the cases this leads to the partial differential equations, for the solution of which numerical methods are necessary to use. The term Model is mainly understood as an ensemble of equations which describe the variables and interrelations of a physical system or process. Developments in computer technology and related software have provided numerous tools of increasing power for specialists in mathematical modelling. One finds a variety of these used to obtain the numerical results of the book.

InTech Europe
University Campus STeP Ri
Slavka Krautzeka 83/A
51000 Rijeka, Croatia
Phone: +385 (51) 770 447
Fax: +385 (51) 686 166
www.intechopen.com

InTech China
Unit 405, Office Block, Hotel Equatorial Shanghai
No.65, Yan An Road (West), Shanghai, 200040, China
中国上海市延安西路65号上海国际贵都大饭店办公楼405单元
Phone: +86-21-62489820
Fax: +86-21-62489821